

Corrosion Protection of Copper Foil by Ni-W Electrodeposited Coating in Kaolin Slurry

Chien-Hung Lin*, Pei-Jing Teng

Department of Physics, ROC Military Academy, Feng-Shan, Kaohsiung 830, Taiwan

*E-mail: linhungcma@gmail.com

Received: 4 April 2020 / Accepted: 1 April 2021 / Published: 30 April 2021

The electrodeposited Ni-W layer was coated on a Cu substrate, and the plating bath was treated with a nickel sulphate solution. The corrosion resistance of the coating layer was evaluated using a corrod-kote test with 1-20 repetitive cycles, and the SSRT (slow strain rate test) was employed to characterize the mechanical properties of the Ni-W layer on the Cu substrate. In the ambient atmosphere, the tensile strength of the Cu substrate with and without Ni-W coating were 285 MPa and 240 MPa, respectively. Moreover, the strength of Ni-W coating was gradually reduced to the minimum value (250 MPa) over 20 cycles in the corrod-kote environment. The fracture surface was observed by scanning electron microscopy (SEM), and the Ni-W coating demonstrated ductile-type fracture and partial brittle cleavage due to its quasi-cleavage features. As the potentiodynamic polarization, the corrosion current densities of the bare Cu with and without Ni-W coating in the presence of the corrod-kote environment were 8.97×10^{-6} and 1.84×10^{-4} A/cm², respectively. Hence, the Ni-W coating layer significantly decreased the corrosion current density of the Cu substrate by 1 order of magnitude. Consequently, the SSRT results completely corresponded to the polarization test results in the corrod-kote environment. The aim of the work presented in this paper was to investigate the strain effect through the Ni-W coating layer in the corrod-kote environment.

Keywords: Ni-W layer, slow strain rate testing (SSRT), corrod-kote test, fracture surface

1. INTRODUCTION

The initial purpose and scope of the surface treatment was the decoration that converted a widely available matrix for an excellent application. The novel trend of the coating technique was towards the superior properties, such as toughness [1-5], corrosion resistance [6-10], conductivity, and environmental manufacture. The corrosion resistance due to the decorative electrodeposition of a nickel coating has been extensively applied to weapon systems, automotive equipment, aviation, the petrochemical industry and electronics manufacture [11-15].

The Ni-W coating enhanced the superior strength of the plated layer over the matrix by DC (direct current) electrodeposition [16]. The composition and hardness of the coating layer were 20 wt % tungsten and 685 HV to the interface, respectively, while citric acid was mixed with chemical reagents in a nickel sulphate solution. The hardness increased with the heat treatment time during incubation in the 723 K vacuum chamber for 24 hours. Furthermore, the nanocrystalline Ni-W grain structure (between 2.5 and 3.5 nm) enhanced the mechanical properties of the specimen during the tensile test. The Ni-W alloy was also plated on the specimen to strengthen the mechanical properties of the substrate [17]. The mechanical performance of the coating layer also involved the grain size, thickness and chemical composition, and the microstructure changed with deposition time for the Watts bath. The coating layer demonstrated superior performance with a thickness of up to 21 μm , and the thickness of the Ni-W coatings increased linearly with exposure time. Although a smoother surface was obtained with the increasing time, the hardness values decreased with the thickness of the Ni-W layer. The toughness of the bare Cu was certainly strengthened due to the Ni-W alloy layer, and the dislocation movement was inhibited in the adjacent interface. The tensile test (strain rate 3.3×10^{-4}) was employed to investigate the fundamental performance of the Cu foil with a rolling test [18]. The strength of the foil with the rolling process and electrodeposition process were 463 and 223 MPa, respectively. Additionally, the elongation rate of the Cu foil was significantly superior to that of others due to the homogeneous grains existing on the specimen after the electrodeposition process. The relationship between the grain size and mechanical properties of the Ni-W coating was discussed [19], and the grain size was classified as coarse grain, nanocrystalline grain ($< 100 \text{ nm}$) and ultrafine grain ($100 \text{ nm} < \text{grain} < 1 \mu\text{m}$). The inverse Hall-Petch relationship was proven when the grain size approached the nanostructure, and the coarse grain size increased with the elongation rate. Hence, the excellent performance for the coating layer was suggested to modify the bimodal grain sizes as a present result.

The manipulator parameters, such as the current efficiency and pH value (8.7 and 9.5), in the plating bath significantly influenced the microstructure of the plating layer [20]. The electrodeposition efficiency and tungsten content increased with the current density, ranging from 0.01 to 0.1 A/cm^2 . Furthermore, the coating layer was stable when it existed in the plating bath (pH= 9.5), and the spherical size (1.5 μm to 3 μm) increased with the current density (0.01-0.05 A/cm^2). The power supply with pulse current was also used in an attempt to coat the Ni-W alloy onto Cu substrates [21]. Additionally, the electrochemical reaction was performed with an intermittent waveform of pulse current, yet the traditional electrodeposition operated in a continuous mode with a direct current (DC) supply. Therefore, the result indicated that the concentration gradient issue could be efficiently overcome by a pulsed current supply because the cation diffused onto the substrate with slow kinetics. Hence, a smoother plane was exhibited, and the duty cycle parameter coordinated with the concentration diffusion. The intermittent power supply between the deposited process with 50% On-Time and 20 Hz frequency significantly enhanced the strength of the substrate. The Ni-W alloy coating was also obtained while the sodium tungstate and nickel sulphate were added in a Watts plating bath by direct current electrodeposition [22]. The tungsten element significantly inhibited the grain growth, and the homogeneous grain was demonstrated within the coating after heat treatment at 400°C. The annealed Ni-W alloy exhibited superior strength and elongation rate over those of the pure Ni coating. Moreover, the corrosion resistance of the Ni-W alloy and pure Ni was evaluated, and the corrosion potential of the

pure Ni negatively shifted toward that of the Ni-W alloy. The passive film on the annealed Ni-W alloy was stable while it was in the 3.5 wt % NaCl.

The objective of this paper was to investigate the corrosion resistance of the coated Ni-W alloy in the mud environment. Moreover, the DC electrodeposition was used to plate the Ni-W alloy on the Cu substrate before the environmental test. The thin coating layer improved defects of the Cu substrate in areas such as the tensile strength and corrosion resistance. Therefore, the tensile performance of the Ni-W alloy was evaluated in the corrodkote solution. This achievement warranted the development of the Ni-W coating while the protective film was observed on the Cu substrate in the mud environment.

2. EXPERIMENTS

2.1 Specimen preparation

The present material of this study was pure copper, and the nominal chemical composition was 99 wt % Cu. The main dimensions of the Cu substrate were (200 mm×20 mm×0.3 mm), which were consistent with the ASTM E345 standard, as shown in Fig. 1.

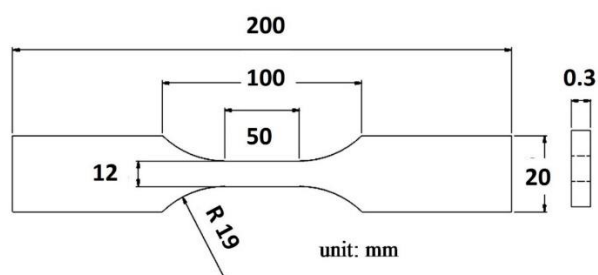


Figure 1. Dimensions (20 mm width by 200 mm length) of the Cu substrate employed for the SSRT (slow strain rate test).

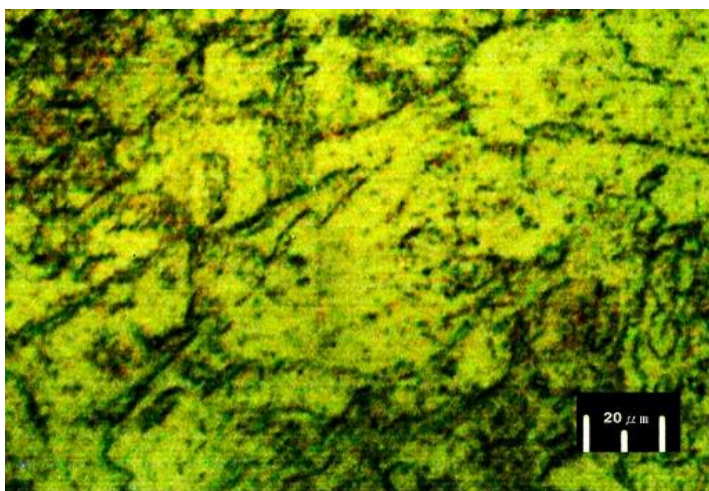


Figure 2. Metallurgical micrograph of the bare Cu surface. The Cu substrate was pre-treated with acid solution (50 vol % HCl) at ambient temperature for 2 min and then rinsed with deionized water. The metallographic structure of the bare Cu is shown as Fig. 2.

2.2 Electrodeposition

Nickel sulphate (0.06 M) and sodium tungstate (0.18 M) were added to a one-litre beaker as sources of Ni and elemental W, and the details of the electrodeposition system are described in Table 1.

Table 1. Composition in the plating bath for the Ni-W alloy.

Constituent	Quantity(Mole/L)
nickel sulfate, NiSO ₄	0.06
sodium tungstate, Na ₂ WO ₄	0.18
sodium citrate, Na ₃ C ₆ H ₅ O ₇	0.3
ammonium chloride, NH ₄ Cl	0.6

The plating bath temperature, current density and pH value were set at 70°C, 5 ASD and 8.5, respectively. The commercial nickel plate (99 wt %) served as the anode and the reaction area (70 mm×30 mm) opposed to the Cu substrate.

2.3 Corrodkote test

The corrodkote test is a rapid and effective technique to evaluate the corrosion resistance of the decorative coating [23]. The reagent grade 2.5 g cupric nitrate, 2.5 g ferric chloride and 50 g ammonium chloride were individually diluted in a 500-ml beaker according to the ASTM B380-97 standard. Then, 30 g kaolin was stirred into the solution consisting of 7 ml cupric nitrate solution, 33 ml ferric chloride solution and 10 ml ammonium chloride solution. The corrodkote slurry was coated on the specimen at a thickness of 1 mm and then dehydrated at room temperature for 1 hour. Then, the specimen was exposed to the test chamber, and the humidity and temperature of test chamber were 38°C and 85%, respectively. The single cycle test lasted for 20 hours before the extraction. Finally, the subsequent SSRT (strain rate of $2.5 \times 10^{-5} \text{ sec}^{-1}$) was conducted in the chamber with the full slurry after the cycle test (1, 5, 10, 15 and 20). The experimental apparatus to evaluate in situ corrosion of the specimen is shown in Fig. 3.

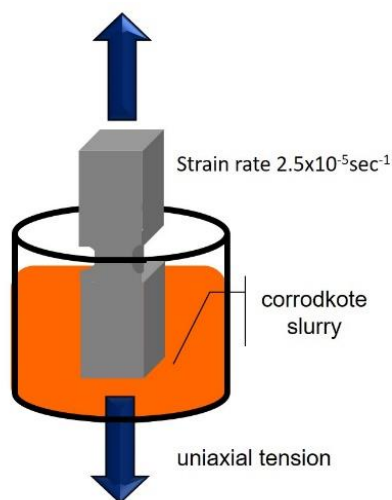


Figure 3. Schematic diagram of the experimental apparatus for the SSRT test.

2.4 Electrochemical Test

The corrosion resistance of the as-deposited specimen were tested in a 50 vol % corrodkote solution with deionized water. The potentiodynamic polarization and AC impedance were provided by a Versastat 4 system (AMETEK Inc.) at ambient temperature. The platinum electrode and an Ag/AgCl electrode were employed as the auxiliary electrode and reference electrode in the experiment, respectively. The as-deposited specimen were exposed to the electrolytic cell as working electrodes. Meanwhile, the potential range and scan rate during the potentiodynamic polarization test were set to -0.5 V to 0.1 V and 0.5 mV/sec, respectively. According to the potentiodynamic polarization, the corrosion potential and corrosion current were employed to analyze the corrosion resistance of the working electrode.

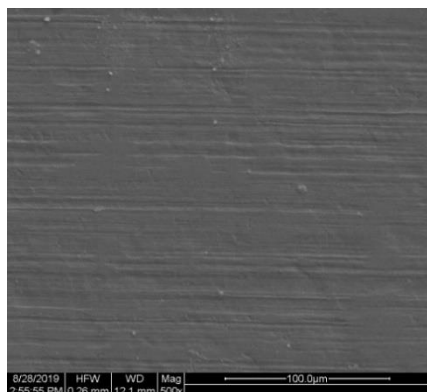
3. RESULTS AND DISCUSSION

3.1 Morphology and composition of the coating

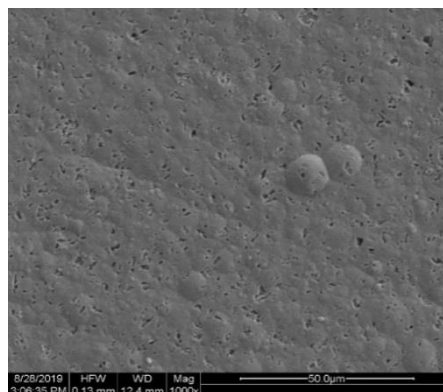
The DC electrodeposited process was used to plate the Ni-W alloy on a Cu substrate. The nickel ion adhered densely to the defect region to promote the adhesion of the nucleus to the substrate [16-17, 20]. Meanwhile, the thickness of the coating increased with the plating time, and the coating layer uniformly incubated on the rough surface of the substrate as shown in Fig. 4(a). The nickel and tungsten ion co-deposited on the Cu substrate to show a nodular structure with voids on the coating as shown in Fig. 4(b). The thickness of the Ni-W coating layer was 25 μm , as shown in Fig. 4(c). The chemical composition of the Ni-W coating was analyzed by energy dispersive spectrometer (EDS), and the W element content was 18.9 wt %.

Atomic force microscopy (AFM) was employed to explore the morphology of Ni-W coating layer as shown in Fig. 5. The grain distributed homogeneously on the surface, and the grain size was

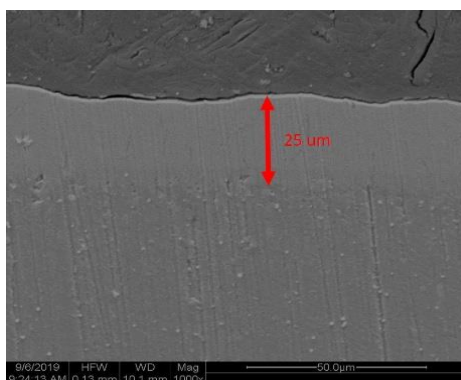
0.5-2 μm . The Ni-W coating demonstrated a smooth property on the surface, and the maximum roughness deviation was $R_{\text{max}} = 380 \text{ nm}$ in the line profile. There were a few defects, such as cracks, pinholes and impurities, embedded on the Ni-W coating [7]. Furthermore, the hardness was examined by the hardness tester (DM2D, AFFRI Inc.).



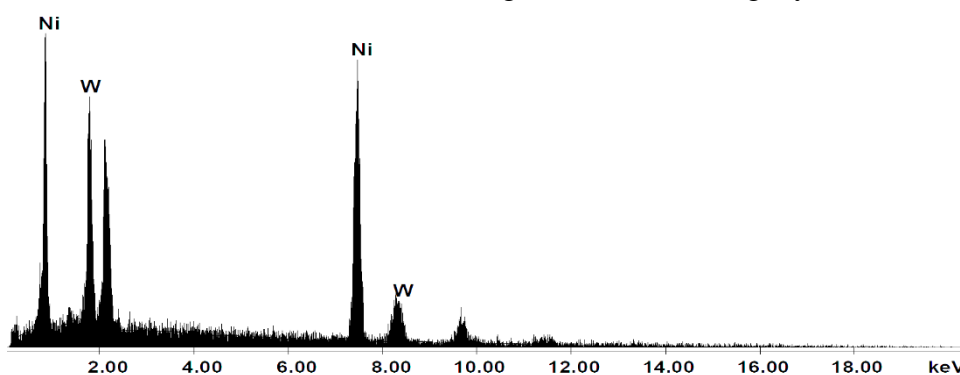
(a) Morphology of bare copper.



(b) Morphology of Ni-W coating.



(c) Cross-sectional SEM images of Ni-W coating layer.



(d) EDS mapping result of Ni-W coating layer.

Figure 4. Scanning electron micrographs of the surface morphology, cross-sectional view and energy dispersive spectrometer mapping for the specimen.

A diamond pyramid was pressed on the surface to examine the Vickers hardness of the specimen, while the standing time and feasible force were 20 seconds and 0.3 kgf, respectively. The average Vickers hardness of the Cu substrate and Ni-W coating layer were 79.6 and 212.6 for every 5 points [15]. The Ni-W coating was proven to effectively enhance the hardness on the Cu substrate, as shown in Table 2.

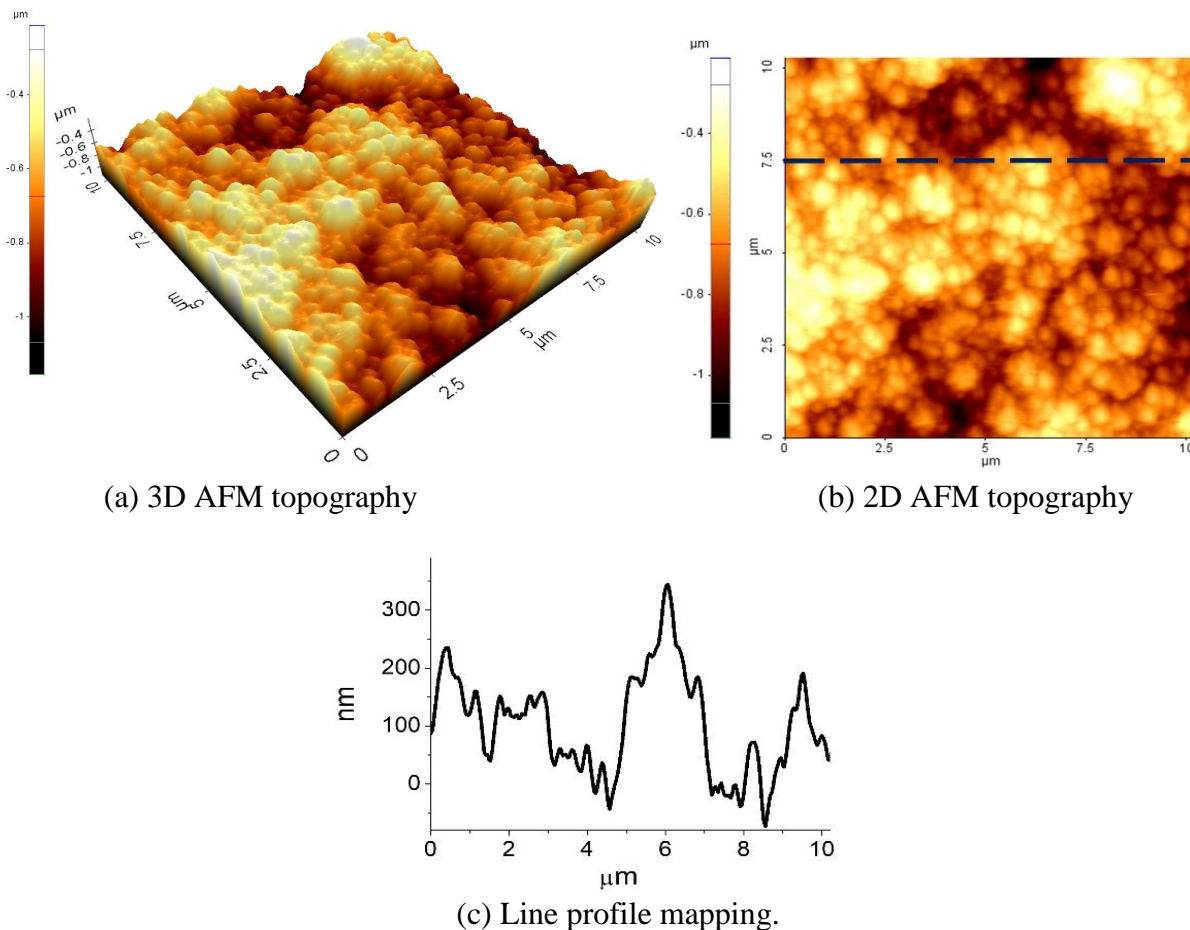


Figure 5. Topography image measured by AFM (atomic force microscopy) and line profiling of Ni-W coating layer.

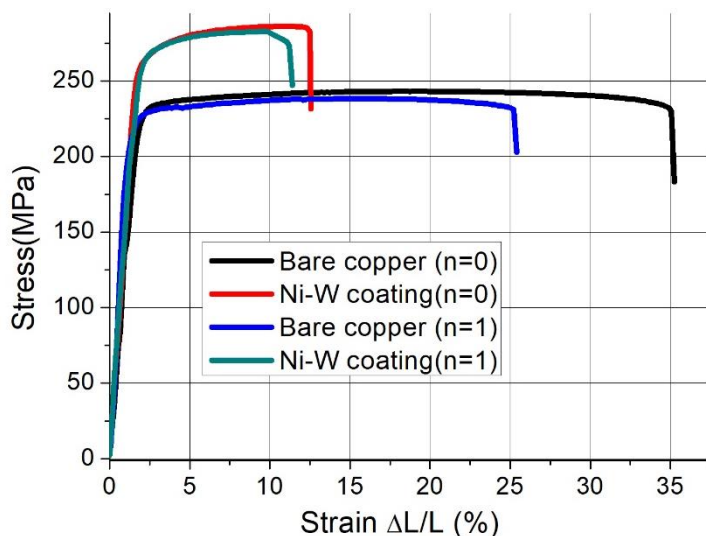
Table 2. List of hardness values for the Cu substrate and Ni-W coating layer. Unit: HV

Exp	1	2	3	4	5	Mean value (HV)
Cu substrate	80.9	79.4	80.0	78.7	79.1	79.6
Ni-W Coating	260.9	26.0	265.1	252.2	258.8	212.6

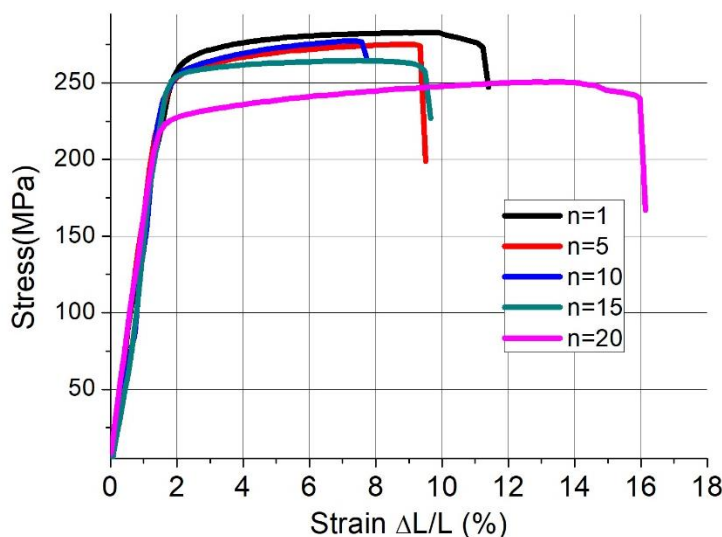
3.2 Constant strain-rate experiment

The yield strength was a crucial criterion for the slip band movement within the specimen under dynamic load. At the end of the plastic deformation stage, a ductile rupture was observed after extensive

deformation [19]. The strength of the Ni-W coating layer and Cu substrate were 285 MPa and 240 MPa, respectively. The Ni-W coating effectively enhanced the strength of the Cu substrate by approximately 18% after the electrodeposition treatment as shown in Fig. 6(a).



(a) Cu substrate with and without Ni-W coating.



(b) Electrodeposited Ni-W coating.

Figure 6. Tensile properties obtained for the specimen exposed to the corrodokote environment with various life cycles. *n indicates number of life cycles with corrodokote test (n = 0, 1, 5, 10, 15, 20).

The maximum strength of the specimen was proven to increase with the coating layer [16, 17-19]. Furthermore, the failure strength of the Ni-W coating degraded within the corrodokote cycle life. The strength of the Ni-W coating was gradually decreased to the minimum value (250 MPa) as shown in Fig. 6(b). The strength of the Ni-W coating decreasing with the cycle life is presented in Table 3. Obviously, the elongation rate exhibited a sharp increase while the Ni-W coating was incubated in a corrodokote

environment for 20 cycles. We concluded that the ductile properties of the Cu substrate were stable, and the Ni-W coating layer decreased the protective mechanism in a corrodkote environment.

Table 3. List of strengths for the specimen during the SSRT in a corrodkote solution (deformed at strain rate of $2.5 \times 10^{-5} \text{ sec}^{-1}$). Units: MPa

Specimen	Corrodkote cycle					
	0	1	5	10	15	20
Cu substrate	240	233	-	-	-	-
Ni-W Coating	285	280	270	273	262	250

3.3 Fracture surface analysis

The strength of the Ni-W coating decreased with the cycle life while it incubated in the corrodkote environment as described in section 3.2. The rupture behaviour was investigated by SEM, as is shown as Fig. 7. The ductile rupture of the Cu substrate accompanied the discrete cavities as exhibited on the necking region [17-18]. Apparently, the cavities accumulated while the crack spread to the surface [19]. The plastic deformation of the Cu substrate was caused by substantial absorbed energy during the uniaxial tension. The cup and cone shape of the Cu substrate was shown as the sequence of the rupture surfaced in Fig. 7(b). Conversely, the rupture surface transitioned from ductile to brittle under the SSRT test, which corresponded to the strain rate of the Ni-W coating (range 8-16%) as described in section 3.2. Hence, the rupture surface was mainly shown as the cleavage plane, and the degree of corrosion intensified with the chronological cycle [17]. The number of dimples decreased through the rupture surface as shown in Fig. 7 (b-d).

The Ni-W coating layer completely lost its protective ability when the corrodkote test reached 20 cycles, and the ductile properties of the Cu substrate with Ni-W coating increased with the elongation rate (16%). Moreover, the invalid Ni-W coating layer resulted in a deeper dimple depth and inferior strength after the corrodkote test, as shown in Fig. 7(f). The present results indicated that second phase particles were observed on the fracture surface due to the ductile behaviour of the Ni-W coating with a 20-cycle test. The effect of ductility on the Ni-W coating showed that the strength was reduced due to corrosion within the coating layer. In the corrodkote environment, the Ni-W coating demonstrated a partial brittle cleavage fracture and a ductile type fracture due to quasi-cleavage features. The morphology of the Ni-W coating surface adjacent (0.5 cm) to the fracture was also shown as Fig. 8. The cracks initially grew on the surface, then rapidly propagated to the core of the matrix. The strain energy was released by the expansion in the microcrack length; the microcrack propagated perpendicularly to the direction of tensile axis. The irregular width of the cracks was approximately 100 μm .

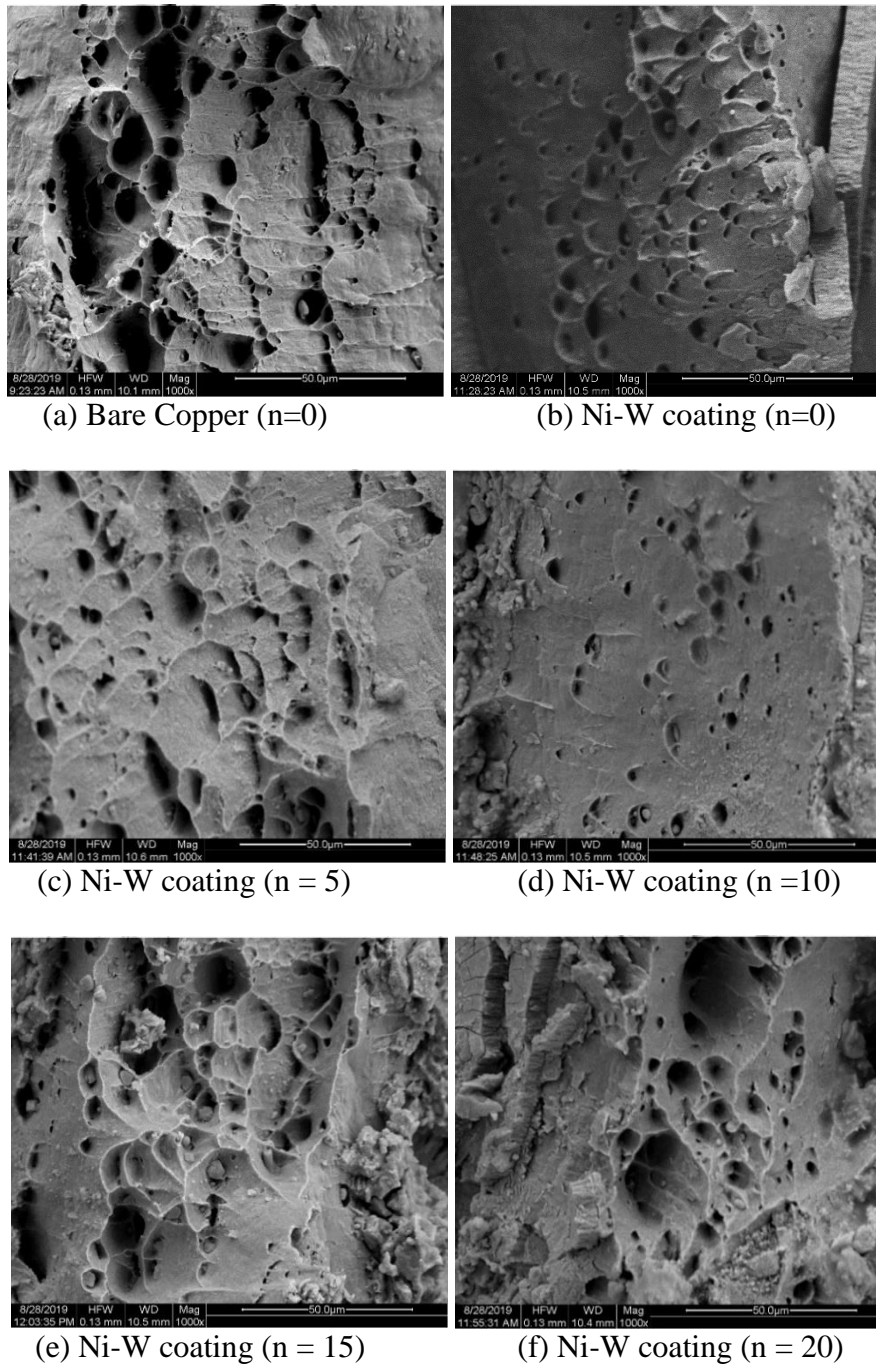


Figure 7. Fracture morphology of the specimen after SSRT (deformed at strain rate of $2.5 \times 10^{-5} \text{ sec}^{-1}$). (a) Cu substrate in an ambient environment; (b-f) the Ni-W coating with various life cycles in the corrodokote environment. *n indicates number of life cycles with corrodokote test (n = 0, 5, 10, 15, 20).

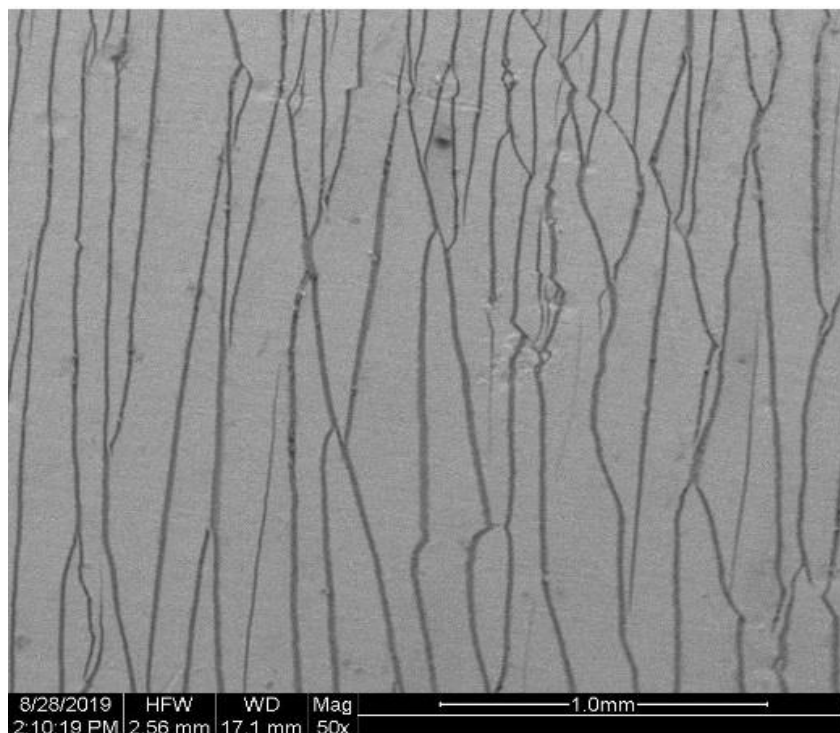


Figure 8. Metallurgical micrographs of the surface adjacent (0.5 cm) to the fracture area of Ni-W coating with 25 μm thickness.

3.4 Corrosion resistance

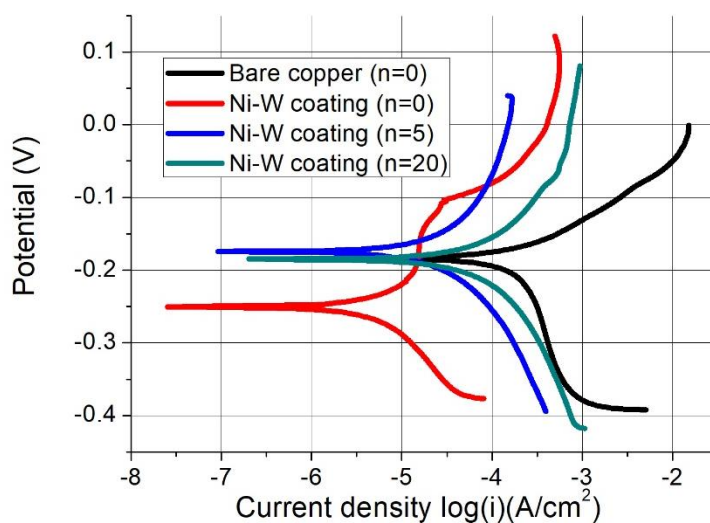


Figure 9. Polarization curves of the Cu substrate with and without Ni-W coating at different cycles of exposure in 50 vol % corrodokote solution. *n indicates number of life cycles with corrodokote test (n = 0, 5, 20).

The potentiodynamic polarization curves obtained for the Cu substrate with and without Ni-W coating are shown in Fig. 9. The Cu substrate coated with the protective layer shifts E_{corr} towards negative values and reduces the I_{corr} (corrosion current density) of the Cu substrate by 1 order of magnitude . The

presence of chloride in the corrodokote test significantly increased the corrosion current of Ni-W coating. Hence, the coating layer transitioned to the localized anode while the galvanic corrosion developed in the corrodokote environment. The E_{corr} of Ni-W coating positively shifted with anodic dissolution and galvanic corrosion in the electrochemical reaction. Fig. 9 shows that the corrosion current densities of Cu substrate with and without Ni-W coating are 8.97×10^{-6} and 1.84×10^{-4} A/cm², respectively. The corrosion potential E_{corr} and corrosion current density i_{corr} characterize the relevant properties responsible for the corrosion resistance of specimens as listed in Table 4. Hence, the present results indicate that the Ni-W coating effectively enhances the corrosion resistance of the Cu substrate [7-8, 20].

Table 4. Corrosion characteristics of Cu substrate with and without Ni-W coating under the corrodokote environment by polarization measurements. *n indicates number of life cycles with corrodokote test (n = 0, 5, 20).

Specimen	n	E_{corr} (V) vs SCE	I_{corr} (A/cm ²)
Cu substrate	0	-0.185	1.84E-4
Ni-W coating	0	-0.253	8.97E-6
	5	-0.169	3.52 E-5
	20	-0.181	7.22 E-5

A perturbation AC signal of 10 mV was used to investigate the impedance response of the working electrode. The increase in the electrochemical impedance magnitude was constant for a frequency range from 0.03 Hz to 20 kHz. The data obtained from the specimen within the corrodokote environment were fitted by the mathematical model as shown in Fig. 10. The R_s was the whole resistance of the electrolyte solution and the contact resistance of the working electrode/wire in physics. Moreover, the low-frequency semicircle extended to the real axis in the impedance response to describe the sum of R_{ct} and R_s in the corrosion reaction as shown in Fig. 11. A Bode plot was employed to explain the frequency behaviour of the Cu substrate with and without Ni-W coating, and the amplitude of the impedance response is shown in Fig. 12.

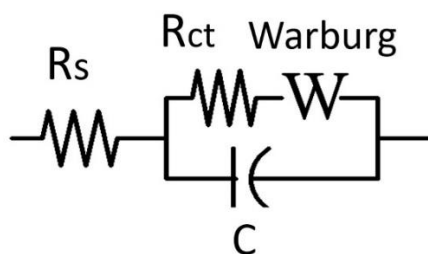
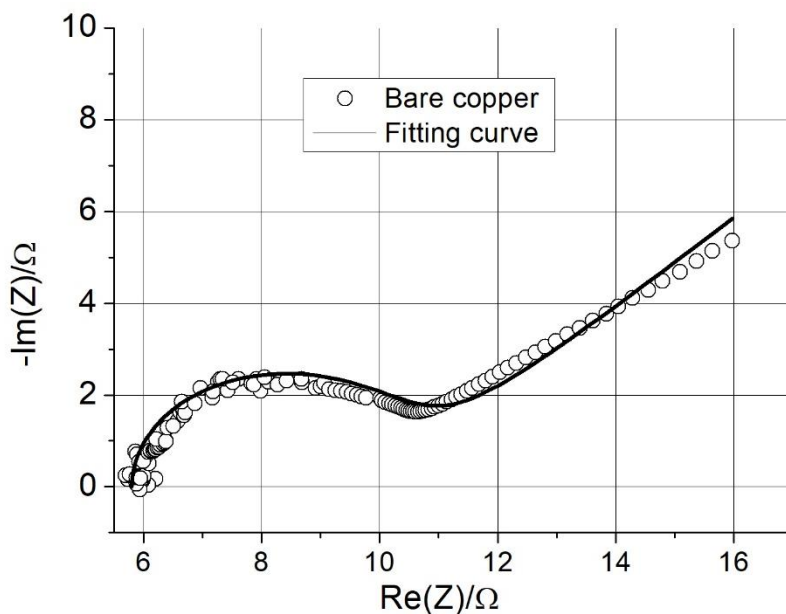
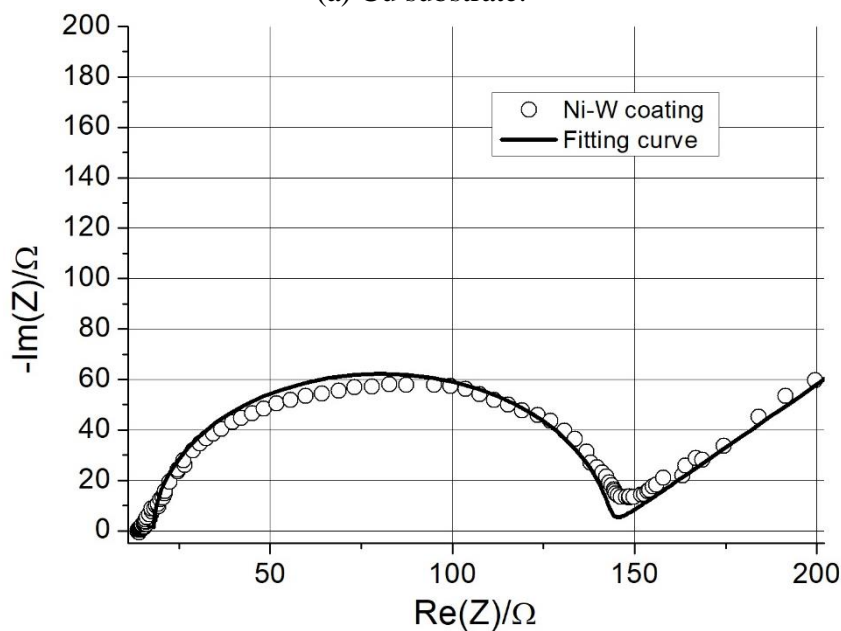


Figure 10. Equivalent circuit used for the fitting data of the impedance response.



(a) Cu substrate.



(b) Ni-W coating.

Figure 11. Nyquist curve of the Cu substrate with and without Ni-W coating exposure in 50 vol % corrodekote solution.

There was a single semicircle in the impedance response plot, then a straight line progresses with an approximately 45° slope in the low frequency region. The high frequency arcs of the Cu substrate with and without Ni-W coating were intercepted with the real axis as R_s at 18.3 and 5.8 Ω , respectively. The R_{ct} of the Cu substrate with and without Ni-W coating were 124.3 and 4.5 Ω , respectively, which represent the kinetic resistance of the corrosive reaction for the working electrode in Table 5.

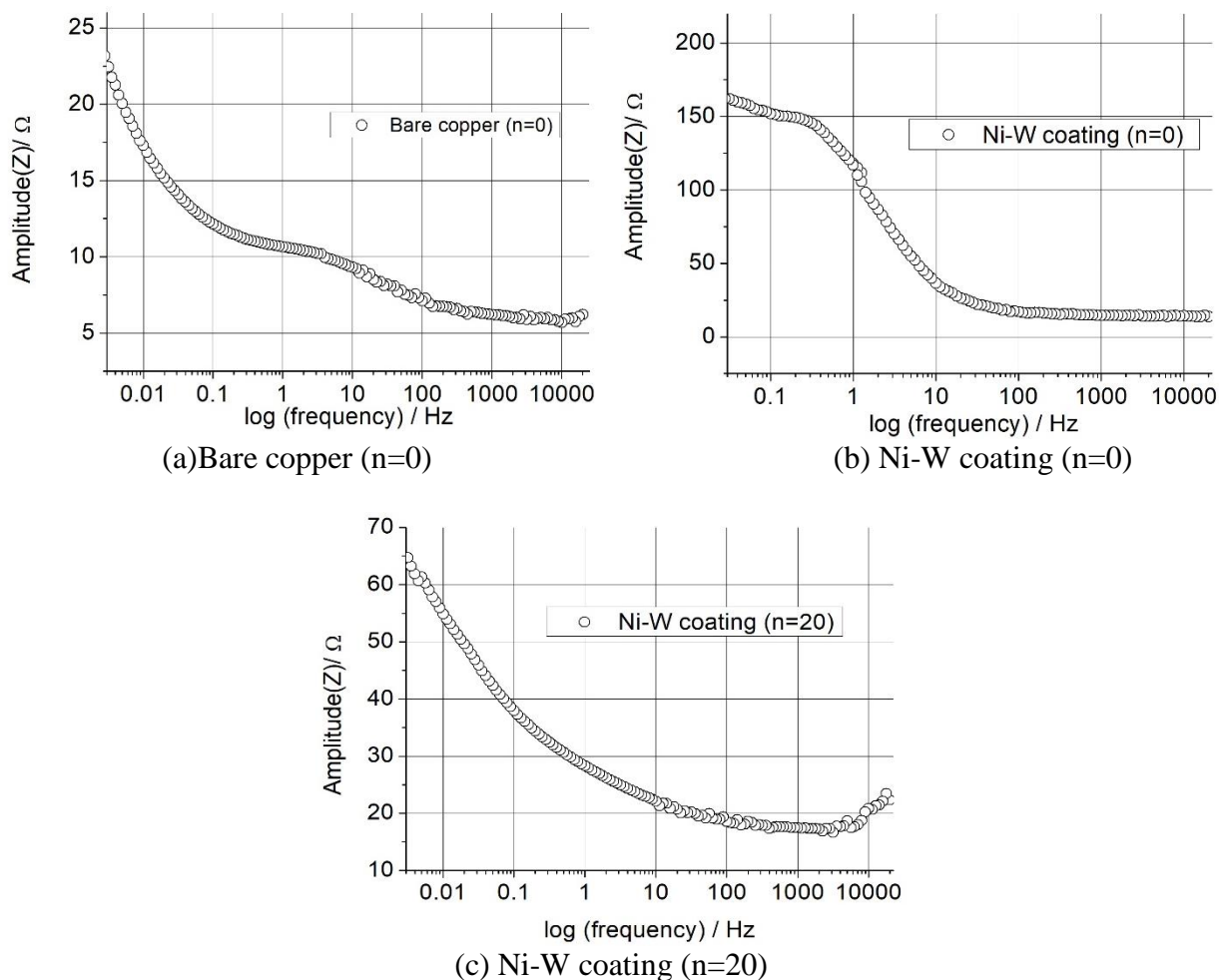


Figure 12. Bode plot of Cu substrate with and without Ni-W coating exposure in 50 vol % corrodekote solution. *n indicates number of life cycles with corrodkote test (n = 0, 20).

Table 5. Fitted result of the EIS spectra for the Cu substrate with and without Ni-W coating.

Specimen	Rs(Ω)	Rct(Ω)	C(F)	Warburg
Cu substrate	5.8	4.5	3E-2	0.8
Ni-W coating	18.3	124.3	3E-5	6.2

The electric double layer over the interface for the working electrode and the charge transfer resistance in the electrochemical reaction were denoted as C and Warburg resistance, respectively. The abundant electronics accumulate on the electric double layer surface and enhance the capacitance effect on the Cu substrate. Furthermore, the Warburg resistance increases with the thickness of the protective layer as Ni-W alloy is plated on the Cu substrate [13, 21]. The Bode diagrams corresponding to the magnitude of the impedance response are shown as Fig. 12. The low-frequency impedance of the Cu substrate with and without Ni-W coating at 3×10^{-2} Hz was 160.8 Ω and 22.6 Ω, respectively. Moreover, the inferior impedance value was obtained on the Ni-W coating during the corrodkote test for 20 cycles,

as shown in Fig. 12(c). According to the fitting data, the magnitude of the impedance response was proven to be significantly related to the corrosion resistance of the specimen [7], and the impedance response decreased when the specimen was exposed to the corrodokote environment.

4. CONCLUSIONS

The mechanical properties of the Cu substrate with and without the Ni-W alloy coating were characterized by the SSRT after the cycle test in the corrodokote environment. The DC electrodeposition process was used to plate the Ni-W alloy on the Cu substrate at a thickness of 25 μm . The Ni-W coating was covered with mud slurry and then exposed in the test chamber. The mud slurry was synthesized using the kaolin and a caustic solution. The temperature and humidity of the cell were fixed at 38 °C and 85%, respectively, for all the experiments. The strength of the Cu substrate with and without Ni-W coating were 285 MPa and 240 MPa, respectively. The Ni-W coating layer completely lost its protective ability when the corrodokote test reached 20 cycles. The strength of the Ni-W coating was gradually reduced to the minimum value (250 MPa) due to the presence of chloride in the corrodokote test. The invalid Ni-W coating layer resulted in a deeper dimple depth on the fracture surface after the corrodokote test. The corrosion current densities of the Cu substrate with and without Ni-W coating were 8.97×10^{-6} and 1.84×10^{-4} A/cm², respectively. The specimen coated with the protective layer significantly decreased the corrosion current density I_{corr} of the Cu substrate by 1 order of magnitude. The low-frequency impedance of the Cu substrate with and without Ni-W coating at 3×10^{-2} Hz was 160.8 Ω and 22.6 Ω , respectively, and the kinetic resistance of the corrosive reaction for the working electrode was enhanced due to the existence of the protective coating. Further research will be performed on the structure of the coating layer (such as its thickness, composition and grain size) for Cu substrate in corrodokote environment.

References

1. C.N. Panagopoulos, G.D. Plainakis, D.A. Lagaris, *Mater. Sci. Eng. B* 176 (2011) 477.
2. J. Liu, X. Zhu, J. Sudagar, F. Gao, P. Feng, *Int. J. Electrochem. Sci.*, 7 (2012) 5951.
3. P.N.S. Casciano, R.L. Benevides, P. de Lima-Neto, A.N. Correia, *Int. J. Electrochem. Sci.*, 9 (2014) 4413.
4. H.T. Wang, J.R. Wang, M.D. Ger, K.H. Hou, *Int. J. Electrochem. Sci.*, 11 (2016) 2419.
5. Y. Hu, Y. Yu, H. Ge, G. Wei, L. Jiang, *Int. J. Electrochem. Sci.*, 14 (2019) 1649.
6. D.B. Lee, J.H. Ko, S.C. Kwon, *Mater. Sci. Eng. A* 380 (2004) 73.
7. K.R. Sriraman, S. Ganesh Sundara Raman, S.K. Seshadri, *Mater. Sci. Eng. A* 460 (2007) 39.
8. X. Liu, Z. Xiang, J. Niu, K. Xia, Y. Yang, B. Yan, W. Lu, *Int. J. Electrochem. Sci.*, 10 (2015) 9042.
9. Q. Niu, Z. Li, X. Yan, G. Liu, B. Wan, *Int. J. Electrochem. Sci.*, 12 (2017) 10259.
10. L. Ma, X. Xi, Z. Nie, T. Dong, Y. Mao, *Int. J. Electrochem. Sci.*, 12 (2017) 1034.
11. C.H. Lin, S.Y. Tsai, *Appl. Energy*. 100 (2012) 87.
12. A. Farzaneh, M.G. Hosseini, S.K. Asl, O. Mermer, *Int. J. Electrochem. Sci.*, 11 (2016) 5140.
13. M. Benaicha, M. Allam, A. Dakhouche, M. Hamla, *Int. J. Electrochem. Sci.*, 11(2016) 7605.
14. Z. Zhang, J. Tang, Y. Wang, M. Apreutesei, H. Wang, *Int. J. Electrochem. Sci.*, 12 (2017) 6180.

15. H.H. Sheu, J.H. Syu, Y.M. Liu, K.H. Hou, M.D. Ger, *Int. J. Electrochem. Sci.*, 13 (2018) 3267.
16. T. Yamasaki, *Mater. Phys. Mech.* 1 (2000) 127-132.
17. C. N. Panagopoulos, E. P. Georgiou, D.A. Lagaris, V. Antonakaki, *AIMS Mater. Sci.* 3 (2016) 324.
18. X.Q. Yin, L.J. Peng, S. Kayani, L. Cheng, J.W. Wang, W. Xiao, L.G. Wang, G.J. Huang, *Rare Met.* 35 (2016) 909.
19. Q. Zhang, Y. Liu, Y.S. Liu, Y.H. Ren, Y.X. Wu, Z.P. Gao, X.L. Wu, P.D. Han, *Mater. Sci. Eng A*, 701 (2017) 196.
20. D.V. Suvorov, G.P. Gololobov, D.Y. Tarabrin, E.V. Slivkin, S.M. Karabanov, A. Tolstoguzov, *coatings.* 8 (2018) 1.
21. I. Matsui, N. Omura, *Mat. Trans.* 59 (2018) 123.
22. J.L. Lv, Z.Q. Wang, T.X. Liang, S.K. Ken, H.D. Miura, *Surf. Coat. Technol.* 337 (2018) 516.
23. H. Koivuluoto, G. Bolelli, A. Milanti, L. Lusvarghi, P. Vuoristo, *Surf. Coat. Technol.* 268 (2015) 224.

© 2021 The Authors. Published by ESG (www.electrochemsci.org). This article is an open access article distributed under the terms and conditions of the Creative Commons Attribution license (<http://creativecommons.org/licenses/by/4.0/>).